

**Interactive comment on “Theoretical framework for estimating snow distribution through point measurements” by E. Trujillo and M. Lehning**

Anonymous Referee #1

Received and published: 29 January 2015

This paper presents estimators for errors of point snow measurements relative to the true mean along transects and within specified areas. Estimators of how representative point measurements are in space are an important topic that so far has received little attention in snow research. The authors assume that snow depth is a random field that exhibits spatial correlation according to an exponential model. From this assumption they estimate the errors by integrating the random variable along transects (1D) and over specified areas (2D).

As far as I can see the derivations are correct.

However, I have difficulties with the way the material is presented. The title suggests that the paper proposes a framework. I do not think this is the case. Instead the paper uses standard geostatistical methods and compares them with snow data. The equations are presented as if they were new, as no references are given. This is misleading as they have been developed by Matheron and colleagues more than half a century ago and can be found in geostatistical textbooks (see eg. Journel and Huijbregts pp. 84 and 117 for the 1D and 2D cases, respectively).

**Response:** *We would like to thank the reviewer for his/her useful comments; they have led to a more clarified introduction, overall presentation of methods and results and an improved discussion. We thank the reviewer for pointing out the reference and the need to acknowledge the previous work in this area, which was not known to us. The references to the works by Matheron and subsequent examples are now included.*

I also have difficulties with the notion that the estimators are specific to snow or hydrologically-relevant variables (p. 24). They apply to ANY random field that is correlated according to an exponential model.

**RE:** *We agree with the reviewer on this point, which is why we refer to the other hydrologic variables as examples in the original manuscript. We have added clarification to this in the Introduction more explicitly in the resubmission to be more emphatic about this.*

*Also, in response to both of these main comments, we have tried to clarify these points in the article from the beginning, as it is not our intention to claim to be the proposers of the first principles of geostatistics that our approach is based on. We have tried to make even more clear and explicit that the motivations of this study are based on what we see as lacking in snow sciences even in the present. Also, we have added references to the researchers and authors that have made contributions in such geostatistical approaches to give appropriate credit. And let us also point out that the derivations are presented for the understanding of the snow community, as so far there have been no examples of these approaches in snow sciences to our knowledge. Evidence of this are the comments by the second reviewer, who suggested the addition of more details about some of the geostatistical principles behind the derivation.*

***The following changes are suggested:***

Change title to something like: “Geostatistical estimation of point measurement errors

- comparisons with snow data”

**RE:** *We have given thorough consideration to the reviewer’s suggestion regarding the title. We have changed the title to “Theoretical Analysis of Errors when Estimating Snow*

*Distribution through Point Measurements” in response to the reviewers suggestion.*

Make it clear that the method is known (and has been known for a long time in fact) and is applied to snow data in this paper. The new contributions of the paper are the comparisons with the snow data but certainly not the equations. Give full credit to the geostatistical literature when presenting the equations and the plots where their numerical values are shown.

**RE:** *Although we were not aware of any derivations that are identical to our equations, the literature the referee has pointed out to us shows a similar approach and is now acknowledged. References to Matheron, Journel and Huijbregts have been added.*

Also say that the kind of variable does not matter in this approach as the variable is fully specified by its variance and correlation scale.

**RE:** *As indicated above, we have now added explicit clarification to this in the Introduction.*

Discuss in more detail what makes the snow application interesting. The cryospheric aspects in the current paper are limited to the shape of the covariance function. For example, it would be of interest how the correlation scale is related to the snow physical characteristics.

**RE:** *In the resubmission, we have added in the Introduction, and Summary and Discussions more explicit reference to how this is mainly directed to snow variables, and how the methodology can be used for the particular case of snow depth and other snow related variables, such as SWE. Discussions of the correlation lengths in snow depth and their relationships to the physical processes have been presented in previous studies, which are referenced throughout the article where appropriate (e.g., Trujillo et al., 2007; Deems et al., 2008; Trujillo et al., 2009).*

With these changes, the paper will be an interesting application of geostatistics to the snow sampling case.

#### References

Journel, A. G. and Huijbregts, C.J. (1978) Mining Geostatistics, Academic Press

#### **References**

Deems, J. S., Fassnacht, S. R., and Elder, K. J.: Interannual Consistency in Fractal Snow Depth Patterns at Two Colorado Mountain Sites, *J. Hydrometeor.*, 9(5), 977-988, doi: 10.1175/2008jhm901.1, 2008.

Trujillo, E., Ramirez, J. A., and Elder, K. J.: Topographic, meteorologic, and canopy controls on the scaling characteristics of the spatial distribution of snow depth fields, *Water Resour. Res.*, 43, W07409, doi: 10.1029/2006WR005317, 2007.

Trujillo, E., Ramírez, J. A., and Elder, K. J.: Scaling properties and spatial organization of snow depth fields in sub-alpine forest and alpine tundra, *Hydrol. Processes*, 23, 1575–1590, doi: 10.1002/hyp.7270, 2009.

1  
2  
3  
4  
5  
6  
7  
8  
9  
10  
11  
12  
13  
14  
15  
16  
17  
18  
19  
20

**THEORETICAL ANALYSIS OF ERRORS WHEN ESTIMATING SNOW DISTRIBUTION  
THROUGH POINT MEASUREMENTS**

By

Ernesto Trujillo<sup>1,2</sup> and Michael Lehning<sup>2, 1</sup>

1. School of Architecture, Civil and Environmental Engineering, École Polytechnique Fédérale  
de Lausanne, Lausanne, Switzerland

2. WSL Institute for Snow and Avalanche Research SLF, Davos, Switzerland

Corresponding Author:

Ernesto Trujillo  
EPFL ENAC IIE CRYOS, Station 2  
Lausanne, Switzerland, CH-1015  
Email: Ernesto.Trujillo@epfl.ch  
Office: +41 21 693 5938

Unknown  
Field Code Changed

Unknown  
Field Code Changed

Unknown  
Field Code Changed

Ernesto Trujillo 2/4/2015 14:48

**Deleted:** THEORETICAL FRAMEWORK FOR  
ESTIMATING SNOW DISTRIBUTION THROUGH  
POINT MEASUREMENTS

24        **Abstract**

25        In recent years, marked improvements in our knowledge of the statistical properties of the  
26 spatial distribution of snow properties have been achieved thanks to improvements in measuring  
27 technologies (e.g., LIDAR, TLS, and GPR). Despite of this, objective and quantitative  
28 frameworks for the evaluation of errors and extrapolations in snow measurements have been  
29 lacking. Here, we present a theoretical framework for quantitative evaluations of the uncertainty  
30 of point measurements of snow depth when used to represent the average depth over a profile  
31 section or an area. The error is defined as the expected value of the squared difference between  
32 the real mean of the profile/field and the sample mean from a limited number of measurements.  
33 The model is tested for one and two dimensional survey designs that range from a single  
34 measurement to an increasing number of regularly-spaced measurements. Using high-resolution  
35 (~ 1m) LIDAR snow depths at two locations in Colorado, we show that the sample errors follow  
36 the theoretical behavior. Furthermore, we show how the determination of the spatial location of  
37 the measurements can be reduced to an optimization problem for the case of the predefined  
38 number of measurements, or to the designation of an acceptable uncertainty level to determine  
39 the total number of regularly-spaced measurements required to achieve such error. On this basis,  
40 a series of figures are presented that can be used to aid in the determination of the survey design  
41 under the conditions described, and under the assumption of prior knowledge of the spatial  
42 covariance/correlation properties. With this methodology, better objective survey designs can be  
43 accomplished, tailored to the specific applications for which the measurements are going to be  
44 used. The theoretical framework can be extended to other spatially distributed snow variables  
45 (e.g., SWE) whose statistical properties are comparable to those of snow depth.

46

## 1 Introduction

47 The assessment of uncertainties of snow measurements remains a challenging problem in  
48 snow sciences. Snow cover properties are highly heterogeneous over space and time and the  
49 representativeness of measurements of snow stage variables (e.g., snow depth, snow density, and  
50 snow water equivalent (SWE)) is often overlooked due to difficulties associated with the  
51 assessment of such uncertainties. This has been, at least in part, due to the limited knowledge of  
52 the characteristics of the spatial statistical properties of variables such as snow depth and SWE,  
53 particularly at the small-scales (sub-meter to tens of meters). However, a turning point has been  
54 reached in recent years thanks to improvements in remote sensing of snow (e.g., light detection  
55 and ranging (LiDAR) and Radar technologies), which have allowed significant progress in the  
56 quantitative understanding of the small-scale heterogeneity of snow covers in different  
57 environments, with resolutions and areas of coverage previously unresolved with the standard  
58 methods of measurement (e.g., Trujillo et al., 2007; Trujillo et al., 2009; Mott et al., 2011).

59 Point or local measurements of snow properties will continue to be necessary for purposes  
60 that range from inexpensive evaluation of the amount of snow over a particular area, to  
61 validation of models and remote sensing measurements. Such measurements have a footprint  
62 representative of a very small area surrounding the measurement location (i.e., support,  
63 following the nomenclature proposed by Blöschl (1999)), and the integration of several  
64 measurements is necessary for a better representation of the snow variable in question over a  
65 given area. Because of this, tools for quantitative evaluations of the representativeness and  
66 uncertainty of measurements need to be introduced, and the uncertainty of such measurements  
67 should be more widely discussed in the field of snow sciences.

68 Currently, efforts to assess the reliability and uncertainty of snow measurements have  
69 focused on statistical analyses using point measurements (e.g., Yang and Woo, 1999; Watson et  
70 al., 2006; Rice and Bales, 2010; Lopez-Moreno et al., 2011; Meromy et al., 2013) or  
71 synthetically generated fields in a Monte Carlo framework (e.g., Kronholm and Birkeland, 2007;  
72 Shea and Jamieson, 2010), and comparisons between remotely sensed and ground data (Chang et  
73 al., 2005; Grünwald and Lehning, 2014). These studies have been useful to empirically quantify  
74 uncertainties associated with point measurements; However, these type of approaches do not  
75 provide a quantitative framework for the assessment of uncertainties associated with a particular  
76 sampling design, they do not allow for an optimal sampling strategy (e.g., selecting the number  
77 of points and locations for a desired accuracy level), and they do not take advantage of the  
78 increased knowledge of the characteristics of the heterogeneity of snow cover properties.

Ernesto Trujillo 2/4/2015 11:18

Deleted: design

79 Another possible approach is one in which the expected error in the estimation of a particular  
80 statistical moment of a field over a defined domain (e.g., areal mean or standard deviation from a  
81 finite number of measurements) is determined on the basis of known statistical properties of the  
82 field in question. Such approach uses geostatistical principles that have been proposed by  
83 Matheron (1955; 1970) and others, and that have been applied in mining geostatistics (Journel  
84 and Huijbregts, 1978), the analysis of uncertainties when measuring precipitation (Rodríguez-  
85 Iturbe and Mejía, 1974), and for a more general analysis of the effects of sampling of random  
86 fields as examples of environmental variables (e.g., Skøien and Blöschl, 2006), among others.  
87 Despite of these examples, there is to the authors' knowledge no attempt of implementing such  
88 type of approach in snow sciences, tailoring the methodology to the particular analysis of  
89 uncertainties when measuring snow variables such as snow depth. Such an implementation  
90 appears to be lacking in numerous studies that use point measurements to represent snow

Ernesto Trujillo 1/4/2015 15:56

Deleted: has been explored for

93 | distribution, addressing the spatial extrapolation of such point measurements as the “true” spatial  
94 | distribution of snow depth when evaluating the performance of interpolation methodologies,  
95 | regressions trees, and hydrological models. These comparisons ignore the intrinsic error incurred  
96 | when extrapolating the original point measurements, leaving a proportion of uncertainty that can  
97 | be significant unaccounted for. This is the principal motivation of the present study, with the  
98 | intention of spreading the use of more objective and quantitative methodologies for error  
99 | evaluation in snow sciences. Also, the approach that is presented below can be used for objective  
100 | survey design to estimate snow distribution from point measurements. We do not intend to  
101 | present our approach as novel in the general geostatistical sense; instead, we present the  
102 | derivation with the specific application for snow sciences in mind. However, because of the  
103 | general nature of the random fields’ theory that the development is based on, similar  
104 | developments can indeed be applied to other environmental variables that can be described as a  
105 | random field.

Ernesto Trujillo 26/3/2015 16:45

**Deleted:** from point measurements

Ernesto Trujillo 1/4/2015 16:12

**Deleted:** Additionally,

Ernesto Trujillo 2/4/2015 11:23

**Deleted:** he development of the expression to evaluate the error presented here includes some additional terms that appear in the derivation of the expression that are not accounted for in developments. These terms are needed to accurately predict the behavior that is observed when measuring snow depth from a limited number of measurements.

106 | On this basis, the error in the estimation of spatial means from point measurements over a  
107 | particular domain (e.g., a profile, or an area) can be quantified as the expected value of the  
108 | squared difference between the real mean and the sample mean obtained from a limited number  
109 | of point measurements. Such an approach, as it will be shown here, uses spatial statistical  
110 | properties of snow depth fields in a way that allows for an objective evaluation of the estimation  
111 | error for snow depth measurements. The sections below illustrate the use of such methodology  
112 | for optimal design of sample strategies in the specific context of snow depth. However, the  
113 | methodology can also be implemented for other snow variables such as snow water equivalent,  
114 | given that similar geostatistics can be used to characterize their spatial organization.

125

## 2 Background

126 Let  $Z(\mathbf{x})$  denote a random field function of the coordinates  $\mathbf{x}$  in the  $n$ -dimensional space  
 127  $\mathbb{R}^n$ . Bold letters represent a location vector from hereon. In our case, the field can represent e.g.:  
 128 snow depth or snow water equivalent (SWE) at a given time of the year. The mean of the process  
 129 over a domain  $A$  (e.g., a profile section or an area) is defined as:

$$130 \quad \mu_z(A) = \frac{1}{A} \int_A z(\mathbf{x}) d\mathbf{x} \quad (1)$$

131 In practice, the mean is often obtained from the arithmetic average of measurements at a  
 132 finite number of locations,  $N$ , within the domain:

$$133 \quad \bar{Z} = \frac{1}{N} \sum_{i=1}^N z(\mathbf{x}_i) \quad (2)$$

134 The performance of the estimator  $\bar{Z}$  can be evaluated by calculating the expected value of  
 135 the square difference between the estimator  $\bar{Z}$  and the true mean  $\mu_z(A)$

$$136 \quad \sigma_{\bar{Z}}^2(A) = E \left[ \left( \frac{1}{N} \sum_{i=1}^N z(\mathbf{x}_i) - \frac{1}{A} \int_A z(\mathbf{x}) d\mathbf{x} \right)^2 \right] \quad (3)$$

137 For a 1<sup>st</sup> order stationary process (i.e., the mean independent of location; e.g., [Cressie \(1993\),](#)  
 138 [section 2; and Journel and Huijbregts \(1978\), section 2](#)), (3) can be expressed as

$$139 \quad \begin{aligned} \sigma_{\bar{Z}}^2(A) &= \frac{1}{N^2} \sum_{i=1}^N VAR[z(\mathbf{x}_i)] + \frac{2}{N^2} \sum_{i=1}^{N-1} \sum_{j=i+1}^N COV[z(\mathbf{x}_i)z(\mathbf{x}_j)] \\ &\quad - \frac{2}{N \cdot A} \sum_{i=1}^N \int_A COV[z(\mathbf{x}_i)z(\mathbf{x}_j)] d\mathbf{x}_j \\ &\quad + \frac{1}{A^2} \int_A \int_A COV[z(\mathbf{x}_i)z(\mathbf{x}_j)] d\mathbf{x}_i d\mathbf{x}_j \end{aligned} \quad (4)$$

Unknown  
Field Code Changed

Unknown  
Field Code Changed

Unknown  
Field Code Changed

Unknown  
Field Code Changed



140 where VAR[ ] and COV[ ] are the variance and the covariance, respectively. If we further  
 141 assume that the process is second order stationary (e.g., Cressie (1993), section 2; and Journel  
 142 and Huijbregts (1978), section 2), that is, if the mean and the variance are independent of the  
 143 location, and the covariance function depends only on the vector difference  $\mathbf{x}_i - \mathbf{x}_j$ , (3) can be  
 144 expressed as

$$145 \quad \sigma_{\frac{z}{2}}^2(A) = \sigma_p^2 \left[ \begin{aligned} & \frac{1}{N} + \frac{2}{N^2} \sum_{i=1}^{N-1} \sum_{j=i+1}^N CORR[\mathbf{x}_i - \mathbf{x}_j] \\ & - \frac{2}{NA} \sum_{i=1}^N \int_A CORR[\mathbf{x}_i - \mathbf{x}_j] d\mathbf{x}_j \\ & + \frac{1}{A^2} \int_A \int_A CORR[\mathbf{x}_i - \mathbf{x}_j] d\mathbf{x}_i d\mathbf{x}_j \end{aligned} \right] \quad (5)$$

146 where CORR[ ] is the correlation function, and  $\sigma_p^2$  is the variance of the point process.

147 The first two terms in (5) are the total sum of the covariances (or correlation as  $\sigma_p^2$  has been  
 148 factored out) between all point locations  $i = 1, \dots, N$  (e.g., measurement locations). The first of  
 149 the two terms is only a function of the number of points, while the second is a function of the  
 150 number of points,  $N$ , and the correlations between the locations. Such correlations are themselves  
 151 a function of the separation vectors (both in magnitude and direction), and the parameters of the  
 152 correlation function. These two terms are independent of the size of the area  $A$ , and can be  
 153 thought of as the portion of the error caused by the correlation between the point processes at the  
 154 locations  $i = 1, \dots, N$  (e.g., measurement locations). Term 3 accounts for the correlation between  
 155 the measurement locations and the continuous process over the domain  $A$ . This term can be seen  
 156 as a negative contribution to the total error assuming that the sum of the integrals is positive. The  
 157 term is a function of the number of points,  $N$ , the domain area,  $A$ , the location of the points and

Unknown  
 Field Code Changed

158 the correlation structure, characterized using the parameters of the correlation function. Lastly,  
159 term 4 is the contribution to the error caused by the intrinsic correlation structure of the  
160 continuous process over the domain. This term is a function of the domain (e.g., size and shape  
161 of  $A$ ) and the correlation structure (e.g., parameters of the correlation function).

### 162 3 Data

163 For the analyses and tests of the methodology presented here, Light Detection and Ranging  
164 (LIDAR) snow depths obtained as part of the NASA's Cold Land Processes Experiment (CLPX)  
165 will be used (Cline et al., 2009). The dataset consists of spatially distributed snow depths for 1-  
166 km x 1-km areas (Intensive Study Areas - ISAs) in the Colorado Rocky Mountains close to  
167 maximum snow accumulation in April, 2003. The data were processed from snow-on (8-9 April,  
168 2013) and snow-off (18-19 September, 2013) LIDAR elevation returns with an average  
169 horizontal spacing of 1.5 m and vertical tolerance of 0.05 m. The final CLPX snow depth  
170 contour product (0.10 m vertical spacing) was generated from these returns. This product was  
171 used to generate gridded snow depth surfaces with 1024x1024 elements over the ISAs, for a grid  
172 resolution of 0.977 m. For this study two areas will be used: the Fraser – St Louis Creek ISA  
173 (FS) and the Rabbit Ears – Walton Creek ISA (RW) (Figure 1). The FS ISA is covered by a  
174 moderate density coniferous (lodgepole pine) forest on a flat aspect with low relief. The RW ISA  
175 is characterized by a broad meadow interspersed with small, dense stands of coniferous forest  
176 and with low rolling topography. The snow depth distributions in these ISAs show differences  
177 that are relevant for the analysis of the methodology introduced here. At the FS ISA, the snow  
178 depth distribution is relatively isotropic (Figure 1b), with short spatial correlation memory and  
179 little variations in the spatial scaling properties (i.e., power-spectral exponents and scaling  
180 breaks) with direction (Trujillo et al., 2007). On the other hand, the spatial distribution of snow

Ernesto Trujillo 31/3/2015 16:07

Deleted: introduced

182 depth in the RW ISA is more anisotropic (Figure 1c), with longer spatial correlation memory  
183 along a principal direction aligned with the predominant wind direction versus shorter memory  
184 along the perpendicular direction, and with variations in the power-spectral exponents and  
185 scaling breaks according to the predominant wind directions (Trujillo et al., 2007).

#### 186 **4 One-dimensional process**

187 The spatial representation of the snow cover requires a basic assumption on the scale or  
188 resolution at which a field or profile is going to be represented. This relies on the spatial support  
189 of the measurements. For the case of snow depths, point measurements from local surveys using  
190 a snow depth probe are frequently used for this representation. Generally, there are additional  
191 sources of uncertainty associated with these types of measurements, such as the accuracy of the  
192 position of the measurement in space or deviations in the vertical angle of penetration of the  
193 probe through the snow pack. These uncertainties are additional to any of the uncertainties  
194 estimated using the methodology discussed here.

195 The one-dimensional case provides a good opportunity to illustrate the limitations of point  
196 measurements. Consider the case of a snow depth profile that is measured using a snow depth  
197 probe at a regular spacing “d”. Each of these point measurements is meant to represent the mean  
198 snow depth over a particular distance surrounding the measurement, and the question is: over  
199 what distance is such assumption valid? In this case, the intrinsic assumption is that the  
200 measurement is representative over the distance “d”, but at this point the validity of such  
201 assumption is not proven.

202 The answer to this question is conditioned to how variable the profile is and over what  
203 distances. To look at this, let us look at two snow depth profiles, one in a forested environment

Ernesto Trujillo 26/3/2015 17:38  
Deleted: at

205 (FS) and another in an open environment (RW) in the Colorado Rocky Mountains (Figure 2a and  
206 Figure 3a, respectively). The variability in the profiles is markedly different, with variations over  
207 shorter distances in the forested area, and a smoother profile in the open and wind influenced  
208 environment. This is reflected in the spatial correlation structure of these snow depth profiles,  
209 with stronger correlations over longer distances in open and wind-influenced environments with  
210 respect to that in forested environments (Trujillo et al., 2007; Trujillo et al., 2009). These  
211 differences should be considered when selecting the sampling frequency required to capture the  
212 variability and accurately represent the mean conditions within a particular sampling spacing.  
213 This is illustrated by comparing the mean snow depth for a particular resolution to the point  
214 value at the center of the interval (Figure 2b in a forested environment and Figure 3b in an open  
215 and wind-influenced environment). In the Figures, average versus point values at several  
216 sampling intervals are compared for normalized profiles ( $\mu = 0, \sigma = 1$ ) separated every 30 m in  
217 both the  $x$  (east) and  $y$  (north) directions and for an area of 500 m by 500 m. The 30-m separation  
218 between profiles is chosen to reduce the spatial correlation between them. Firstly, the resulting  
219 comparison shows that the point values generally overestimate the variability in mean snow  
220 depths if we replace the mean snow depth distribution by its point sample. To clarify this, let us  
221 consider here two snow depth profiles, one with the snow depths at the nominal scale (~1 m),  
222 and a second one with a moving average (MA) of the first one with an averaging window equal  
223 to the sampling spacing. Ultimately, the variance/standard deviation of the first profile (~1 m) is  
224 larger than that of the MA, with a distribution that reflects these differences. The samples drawn  
225 from the first profile will reflect a larger variance than that of the samples from the MA profile as  
226 they are drawn from these distributions, and this is what is reflected in Figure 2 and Figure 3.  
227 The degree of overestimation can be quantified through the slope of the regression line (in red in

228 Figure 2b and Figure 3b). In the forested environment (Figure 2b), the slopes range between 0.8  
229 and 0.13, with decreasing slopes with increasing spacing. These slopes indicate that, on average,  
230 the mean values are 0.8 times the point values for the 5 m spacing and 0.1 times the point values  
231 for the 100 m spacing. In the open and wind-dominated environment, the slopes are higher and  
232 range between 0.97 and 0.23 from 5 m spacing and 100 m spacing, respectively. A clear  
233 difference emerges: forested environments require shorter separation between single  
234 measurements if the snow depth profile is to be accurately captured by the measurements. The  
235 variability within the size of the interval determines the degree of uncertainty associated with the  
236 point measurements, as the sub-interval variability is related to the degree of overestimation of  
237 the mean value within the interval. Secondly, the differences between average and point values  
238 for each spacing distance are generally more scattered in the forested environment than in the  
239 open environment, and in both environments the degree of scattering increases with spacing  
240 (Figure 2c and Figure 3c). However, it is important to note here that we are comparing  
241 normalized profiles ( $\mu = 0$ ,  $\sigma = 1$ ), allowing us to focus on the rescaled spatial variations. What is  
242 highlighted is the relevance of the spatial structure of the profile rather than the absolute  
243 variance. This spatial structure can be quantified by, for example, the spatial  
244 covariance/correlation function.

245 Additionally to the differences in the correlation structure, there are also differences in the  
246 absolute variability in snow depth in these environments (Figure 4). As opposed to the  
247 normalized snow depth discussed above, the subinterval standard deviation as a function of  
248 interval size along the profiles is higher in the open and wind-influenced environment at RW  
249 versus the forested environment at FS (Figure 4a). Mean standard deviation values in the open  
250 environment are twice as large, as those at the forested environment towards the larger interval

Ernesto Trujillo 2/4/2015 11:26

Deleted: T

Ernesto Trujillo 2/4/2015 11:26

Deleted: r

253 sizes (~100 m). The standard deviation increases with interval size in both environments, with  
254 the steepest increase at the lower interval sizes. Furthermore, the standard deviation tends to  
255 stabilize more rapidly in the forested environments, with an increase of only 1.8 cm between 30  
256 m and 100 m. On the other hand, the standard deviation continues to increase in the open  
257 environment at RW, with less of an asymptotical behavior for the scales analyzed.  
258 Complementary, the shaded areas (25% to 75% quantiles) give an idea of the variability of  
259 standard deviation values, with a much wider range in RW versus FS, and an increase in the  
260 range between quantiles with interval size in RW.

Ernesto Trujillo 2/4/2015 11:27

**Deleted:** in within

Ernesto Trujillo 2/4/2015 11:27

**Deleted:** The

261 Consistent with the standard deviation, the sub-interval mean range (range defined as the  
262 difference between the maximum and minimum snow depths within an interval) increases with  
263 interval size in both FS and RW (Figure 4b). However, the mean range is larger in the open  
264 environment at RW and the rate of increase with interval size is also steeper. Similarly, the  
265 shaded areas indicate wider distribution of range values in the open environment at RW, while  
266 relatively uniformly distributed around the mean across interval sizes in the forested environment  
267 at FS. The results in Figure 2-Figure 4 illustrate this contrasting behavior between the snow  
268 covers in these environments and their influence on measurement strategies: that is, the forested  
269 environments requires shorter separation between measurements for accurate representation of  
270 the snow cover, however, in the wind-influence and open environment, the subinterval  
271 variability is higher indicating wider variations around any sampled measurement within the  
272 interval.

Ernesto Trujillo 2/4/2015 11:28

**Deleted:** Also important

Ernesto Trujillo 2/4/2015 11:29

**Deleted:** two compensating

Ernesto Trujillo 2/4/2015 11:29

**Deleted:** differences

273 Ultimately, the number and distance between measurements and the specific arrangement of  
274 the measurements are all conditioned to what the measurements are needed for. Hydrologic  
275 applications may not require a highly detail representation of a snow depth profile (or a field),

281 and representing the average conditions over a given distance (or area) is sufficient, but small-  
282 scale process-based studies may require a more detailed characterization over shorter distances  
283 (or smaller areas). This implies that the decision depends on the particular use that the  
284 measurements will support. In the following sections, the equations presented in the Background  
285 (section 2) will be applied to evaluate the uncertainty associated with multiple measurement  
286 designs for profiles and fields of snow depth.

#### 287 4.1 Case 1: Single measurement along a profile section

288 Equation (2) can be used to evaluate the uncertainty of a single measurement along a profile  
289 section of length  $L$ . For this case, as well as for the following cases in this article, an exponential  
290 covariance with a decay exponent  $\nu$  ( $\nu > 0$ ) will be assumed:

$$291 \quad COV(\mathbf{h}, \sigma, \nu) = \sigma^2 \exp(-\nu \|\mathbf{h}\|) \quad \text{for } \sigma^2 > 0, \text{ and } \nu > 0 \quad (6)$$

292 where  $\sigma^2$  is the variance, and  $\|\mathbf{h}\|$  is the length of the vector  $\mathbf{h}$ . For this one-dimensional case  
293 and combining (6) and (5), the following expression is obtained:

$$294 \quad \sigma_{\frac{z}{2}}^2(x, L, \nu) / \sigma_p^2 = 1 - \frac{2}{Lv} [2 - \exp(-\nu x) - \exp(-\nu \cdot [L - x])] + \frac{1}{L^2 \nu} [2L + \frac{2}{\nu} \exp(-\nu L) - \frac{2}{\nu}]$$

295 (7)

296 where  $x$  is the distance from one extreme of the section to the location of the measurement  
297 (Figure 5a). The normalized squared error  $\sigma_{\frac{z}{2}}^2(x, L, \nu) / \sigma_p^2$  is minimized at  $x$  equal to half of the  
298 section length,  $L/2$ , regardless of  $\nu$ . The existence of a correlation in the profile leads to this  
299 solution, as the middle location contains more information about its surroundings. Also, this  
300 solution is different from the solution for an uncorrelated profile (e.g., white noise), for which

Unknown  
Field Code Changed

Unknown  
Field Code Changed

Ernesto Trujillo 2/4/2015 11:34  
Deleted: the  
Ernesto Trujillo 2/4/2015 11:34  
Deleted: because of the correlation to the surrounding snow depths

304 the squared error would be equal to the variance, independent of the location of the  
305 measurement.

306 The results here are confirmed with an analysis of LIDAR snow depths profiles in FS and  
307 RW (Figure 6). The analysis consists of calculating the difference between the mean and the  
308 point value for sections of a given length (varied between 10 m – 50 m) and for  $x$  (Figure 5a)  
309 between 0 and  $L$  along the profile sections. Each sample section of length  $L$  will provide a single  
310 difference for each of the  $x$  values. These sample differences are then used to calculate the mean  
311 normalized squared error for each  $x$ , and the same is repeated for each section length  $L$ . The  
312 results indicate that the real snow depth profiles behave as predicted by the model of the error,  
313 with a minimum error at  $x$  equal to half of the section length. Another difference highlighted by  
314 these results is the difference between the sample errors in the forested environment (FS) versus  
315 the open environment (RW) for the larger interval sizes (e.g., 50 m). The sampled normalized  
316 squared error in the forested environment shows only a mild decrease in the square error to  
317 around 0.7-0.8 towards the inside of the section length. However, this decrease is achieved for  
318 the measurement along most of the interval length with the exception of the extremes. This can  
319 be explained by the relationship between the spatial memory of snow depth (e.g., the correlation  
320 function) and the section length. Densely forested environments exhibit correlation lengths that  
321 are shorter than those in open and wind influenced environments (e.g., Trujillo et al., 2007;  
322 Trujillo et al., 2009). As the section length increases beyond such correlation lengths, a  
323 measurement location towards the middle of the interval contains less information of the  
324 surrounding snow depths in a forested environment (e.g., FS) versus an open and wind  
325 influenced environment (e.g., RW). This is observed in Figure 6c versus Figure 6f, with the  
326 results in RW showing a more clear minimum towards the center of the profile section. The

Ernesto Trujillo 7/4/2015 11:26

Deleted: Figure 6

Ernesto Trujillo 7/4/2015 11:26

Deleted: Figure 6

Ernesto Trujillo 7/4/2015 11:26

Deleted: Figure 6



330 results also show a poorer performance of the model in RW versus FS, as the exponential  
331 correlation model has a poorer fit in RW at the shorter-lag range; However, model performance  
332 is improved for longer section lengths (e.g., [Figure 6c](#) and [f](#))

Ernesto Trujillo 7/4/2015 11:26

Deleted: Figure 6

333 Model and sampled results thus support that the measurement location can be fixed in the  
334 middle of the interval, and the normalized squared error can then be described as a function of  
335 both, the exponential decay exponent,  $\nu$ , and the length of the section,  $L$  ([Figure 7a](#)). The  
336 normalized squared error increases with interval length, with a steeper increase for larger  
337 exponential decay exponents, for which the squared error approaches that of an uncorrelated  
338 field more rapidly. The theoretical model is tested on the snow depth fields at FS and RW. The  
339 test consists of calculating the sampled normalized squared error as the average of all squared-  
340 differences between the mid-section snow depth and the mean from all LIDAR grid-points  
341 within each interval of length  $L$ . This is done for profiles separated every 30 m, similar to the  
342 analysis above, and for profiles along the  $x$  and  $y$  directions. The theoretical normalized squared  
343 error is estimated from (7) using the exponential decay exponent from the model fitted to the  
344 sampled correlation function. The results show that the theoretical model reproduces the sampled  
345 squared error remarkably well, even reproducing the anisotropic properties of the correlograms,  
346 represented by the different exponents of the exponential model along  $x$  and  $y$  directions ([Figure](#)  
347 [7b](#) and [c](#)). The model also reproduces the different behavior of the squared error between both  
348 fields (i.e., FS and RW), showing that the normalized squared error increases more rapidly and is  
349 larger in the forested environment ([Figure 7b](#)) versus the open environment ([Figure 7c](#)).  
350 However, it should be noted here that as the error is normalized, and as the variance of the field in  
351 the open environment is larger ([Figure 4a](#)), the absolute squared error could reach higher values  
352 in the open environment (RW). In this regard, one feature to discuss here is the assumption that

Ernesto Trujillo 7/4/2015 11:26

Deleted: Figure 7

Ernesto Trujillo 7/4/2015 11:26

Deleted: Figure 7

Ernesto Trujillo 7/4/2015 11:26

Deleted: Figure 7

Ernesto Trujillo 7/4/2015 11:26

Deleted: Figure 7

Ernesto Trujillo 2/4/2015 11:36

Deleted: ,

359 the point variance of snow depth in these environments has been estimated as the spatial variance  
 360 over the entire study area, as it is generally practiced in time series analysis and geostatistics. In  
 361 practice, this is the only possible approach because there is limited information to estimate the  
 362 point variance from multiple realizations of the process at each spatial location, as inter- and  
 363 intra- annual snow depth fields are not available, not only for these areas, but for almost any area  
 364 where this methodology may be applied.

#### 365 4.2 Case 2: Three measurements along a profile section

366 From (5) it is also evident that increasing the number of measurements will reduce the  
 367 squared error. In the case of three measurements separated by a distance 'a', with the middle  
 368 measurement centered in the section of length L (Figure 5b), and for an exponential covariance  
 369 function with parameter v, (5) leads to the following expression for this particular case:

$$\begin{aligned}
 \sigma_z^2(a, L, v) / \sigma_p^2 &= \frac{1}{3} + \frac{2}{9} [2 \exp(-va) - \exp(-2va)] \\
 &- \frac{4}{3Lv} \left[ 3 - \exp\left(-\frac{vL}{2}\right) (1 + \exp(-va) + \exp(va)) \right] \\
 &+ \frac{1}{L^2 v} \left[ 2L + \frac{2}{v} \exp(-vL) - \frac{2}{v} \right]
 \end{aligned} \tag{8}$$

371 Equation (8) can be minimized to determine the optimal separation distance between points,  
 372 a, as a function of L and v:

$$a_{optimal} = -\frac{1}{v} \ln(t) \tag{9}$$

374 where

$$t = \frac{B + \sqrt{B^2 - 4AB}}{2A}$$

Unknown  
Field Code Changed

Ernesto Trujillo 7/4/2015 11:26  
Formatted: Default Paragraph Font  
Ernesto Trujillo 7/4/2015 11:26  
Deleted: (8)

Unknown  
Field Code Changed

377

$$A = \frac{4\nu}{9}$$

378

$$\text{and } B = -\frac{4}{3L} \exp\left(-\frac{\nu L}{2}\right)$$

379

The combination of (8) and (9) can be used to determine the normalized squared error,

380

$\sigma_z^2 / \sigma_p^2$ , and the optimal distance,  $a_{optimal}$ , for the measurement pattern in Figure 5b. The model

381

predicts that the normalized squared error is minimized at an intermediate location between 0

382

and  $L/2$  (black lines in Figure 8a and b). The results show an increase in the error with interval

383

size,  $L$ , as well as little sensitivity of  $a_{optimal}$  to  $\nu$ . This latter feature can be seen as an advantage

384

since small biases in the estimation of  $\nu$  will not result in significant biases in the estimation of

385

$a_{optimal}$ . One could almost assume a value of  $a_{optimal}$  without prior knowledge of the exponential

386

decay exponent, selecting  $a_{optimal}$  within the range of values indicated by the model for a range of

387

possible exponential decay exponents. Note that  $a_{optimal}$  is located close to the 60% distance from

388

the center towards the outer boundary of the profile section for all section lengths (Figure 8a and

389

b). On the other hand, the measurement error displays a higher sensitivity to  $\nu$  around  $a_{optimal}$ ,

390

indicating that biases in the estimation of  $\nu$  would have a more noticeable effect on the

391

estimation of the measurement error. This is further clarified in Figure 8c, in which the

392

normalized error (not squared) and  $a_{optimal}$  can be obtained for corresponding profile section

393

lengths ( $L$ ) and exponential decay exponents ( $\nu$ ) based on the isolines shown. For example, for a

394

profile section of 30 m, and an exponential decay exponent of  $0.2 \text{ m}^{-1}$ , the normalized error is

395

0.32 and  $a_{optimal}$  is 9.63 m (see intersect of the two isolines in Figure 8c). The normalized error in

396

Figure 8c is not squared, highlighting the sensitivity of the measurement error to  $\nu$ , which

Ernesto Trujillo 7/4/2015 11:26

Formatted: Default Paragraph Font

Ernesto Trujillo 7/4/2015 11:26

Deleted: (8)

Ernesto Trujillo 1/4/2015 18:03

Deleted: increasing

Ernesto Trujillo 26/3/2015 18:36

Deleted: to

400 represents the degree of spatial correlation of the profile in this case (e.g., lower values indicate  
401 stronger spatial memory/correlation, hence lower measurement errors).

402 The performance of the model is tested against the normalized squared error obtained from  
403 the same snow depth profiles in FS and RW. The test consists of estimating the normalized  
404 squared error for profiles sections of length between 10 m and 80 m, with  $a$  being varied between  
405 0 and  $L/2$  (Figure 9). For each value of  $a$ , the normalized squared error is estimated based on the  
406 means obtained using the three snow depth samples for each section. All squared differences are  
407 then averaged to obtain the values presented in the Figure. Sampled and modeled errors follow  
408 the same trend across all  $a$  values and for the different  $L$  values in Figure 9. The minimum error  
409 is also reproduced by the model proving the applicability of the model for estimating the optimal  
410 separation between measurements. The model does perform better in the forested environment of  
411 FS versus RW, particularly for lower  $a$  values. This can be justified as the exponential  
412 covariance model displays a better fit in FS over RW, particularly over the lower range of lag  
413 values. Also, note that both the modeled and sampled normalized squared errors are lower for the  
414 snow depth profiles at RW because of the longer spatial memory of the snow depth distribution  
415 in this environment (higher spatial correlations) when compared to that in FS.

### 416 | 4.3 Case 3: $N$ measurements along a profile section

417 As stated above, the measurement error can be reduced by increasing the number of  
418 measurements taken over a given section of length  $L$ . Let us focus on the case of stratified  
419 sampling where  $N$  regularly spaced measurements are taken over the interval (Figure 5c), and to  
420 quantify this reduction we can use (5) and the exponential covariance model. Equation (5) can  
421 then be reduced to:

422

$$\begin{aligned} \sigma_z^2(N, L, \nu) / \sigma_p^2 &= \frac{1}{N} + \frac{2}{N^2} \sum_{k=1}^{N-1} k \exp(-\nu [L - kL/N]) \\ &- \frac{4}{Lv} \left[ 1 - \frac{1}{N} \sum_{k=1}^N \exp\left(-\nu \frac{L}{N} [N - k + 1/2]\right) \right] \\ &- \frac{2}{L^2 \nu^2} [1 - Lv - \exp(-\nu L)] \end{aligned} \quad (10)$$

423

424

425

426

427

428

429

430

431

432

433

434

435

436

437

438

439

440

The normalized squared error ( $\sigma_z^2 / \sigma_p^2$ ) obtained with (10) for profiles sections of lengths between 10 and 80 shows a steep decrease with  $N$  (Figure 10), with a steeper decrease for higher exponential decay exponents. For the longer profile sections (e.g., 80, Figure 10d), little reductions are achieved in the squared error beyond only a few measurements (e.g.,  $N = 16$ ). Equation (10) and the results in Figure 10 can be used to determine the number of measurements necessary to achieve a desired accuracy level. One could, for example, design a survey to sample a snow depth profile with a mean value every 10 m. The number of measurements required to achieve a desired level of accuracy can be obtained from Figure 10a, based on previous knowledge of the sample estimate of the exponential decay exponent. This can be achieved thanks to the intra-annual and inter-annual persistence of the spatial patterns, and hence, the spatial statistical properties of snow depth fields in mountain environments, as shown in previous studies using both manual surveys and LIDAR measurements (e.g., Deems et al., 2008; Sturm and Wagner, 2010; Schirmer et al., 2011; Melvold and Skaugen, 2013; Helfrich et al., 2014). A detailed spatial survey (e.g., dense manual measurements or TLS), sampling different portions of an area can be used to determine the covariance/correlation characteristics of the snow depth distribution, with which the model for the error can be applied. An a priori estimate of the exponential decay exponent may also be possible and will be tested in future applications of the framework, given the relative insensitivity of the error with respect to  $\nu$ .

Unknown  
Field Code Changed

Ernesto Trujillo 7/4/2015 11:26  
Formatted: Default Paragraph Font  
Ernesto Trujillo 7/4/2015 11:26  
Deleted: (10)

Ernesto Trujillo 7/4/2015 11:26  
Formatted: Default Paragraph Font  
Ernesto Trujillo 7/4/2015 11:26  
Deleted: (10)

443 Following the method described in the previous section, we test the performance of the  
444 model against the normalized squared error obtained from the same snow depth profiles in FS  
445 and RW. In this case, the sampled squared error is estimated based on the  $N$  regularly-spaced  
446 measurements distributed along the profile sections of length  $L$ . As the snow depth fields are  
447 gridded at  $\sim 1$ -m resolution, the location of the measurements is approximated to the closest  
448 coordinate in the profile section following the pattern in Figure 5c. Once again, sampled and  
449 modeled errors follow closely the same trend for the different  $L$  values in both FS and RW  
450 (Figure 11). The error decreases with  $N$ , with a rapid decay at the lower  $N$  values, illustrating that  
451 the error can be drastically reduced by simply increasing the number of measurements by a small  
452 amount. The normalized squared error across all  $N$  values is lower for RW than for FS,  
453 consistent with the higher spatial correlations observed in the snow depth fields of RW versus  
454 FS. Once again, there are some differences between the sampled and modeled normalized  
455 squared error in RW for the shorter profile lengths and for small  $N$  values: a consequence of the  
456 poorer fit of the exponential model for the shorter lag range in RW. However, the model is still  
457 able to reproduce the error in both fields, and the applicability of the model is illustrated even  
458 when the fit of the correlation model can be improved.

## 459 **5 Two-dimensional process**

460 Similar to the one-dimensional process, equation (5) can be formulated to calculate the  
461 squared error in the two-dimensional space. To exemplify this, we apply the methodology to an  
462 isotropic process over the  $x$ - $y$  plane for three cases in a square area: (a) one single measurement  
463 in the center of the area, (b) five measurements radiating out from the center (Figure 12a), and  
464 (c)  $N$  by  $N$  measurements regularly spaced in the  $x$  and  $y$  directions (Figure 12b).

465 For the isotropic case, the covariance/correlation function is only dependent on the  
 466 magnitude of the lag vector,

$$467 \quad h_{i,j} = |\mathbf{x}_i - \mathbf{x}_j| \quad (11)$$

468

469 and, consequently, the error is represented by,

$$470 \quad \sigma_{\frac{z}{2}}^2(A) = \sigma_p^2 \left[ \begin{aligned} & \frac{1}{N} + \frac{2}{N^2} \sum_{i=1}^{N-1} \sum_{j=i+1}^N CORR[h_{i,j}] \\ & - \frac{2}{NA} \sum_{i=1}^N \int_A CORR[h_{i,j}] d\mathbf{x}_j \\ & + \frac{1}{A^2} \int_A \int_A CORR[h_{i,j}] d\mathbf{x}_i d\mathbf{x}_j \end{aligned} \right] \quad (12)$$

471

472 The exponential correlation function for the isotropic case takes the following form:

$$473 \quad CORR(h,v) = \exp(-vh) \quad (13)$$

474 where  $h$  is the magnitude of the lag vector. Replacing into the expression for  $\sigma_{\frac{z}{2}}^2$ , we obtain,

$$475 \quad \sigma_{\frac{z}{2}}^2 = \sigma_p^2 \left[ \begin{aligned} & \frac{1}{N} + \frac{2}{N^2} \sum_{i=1}^{N-1} \sum_{j=i+1}^N \exp(-v|\mathbf{x}_i - \mathbf{x}_j|) \\ & - \frac{2}{NA} \sum_{i=1}^N \int_A \exp(-v|\mathbf{x}_i - \mathbf{x}_j|) d\mathbf{x}_j \\ & + \frac{1}{A^2} \int_A \int_A \exp(-v|\mathbf{x}_i - \mathbf{x}_j|) d\mathbf{x}_j d\mathbf{x}_i \end{aligned} \right] \quad (14)$$

476 For the case of a rectangular area of side dimension  $L_x$  and  $L_y$  in the corresponding  $x$  and  $y$   
 477 directions, the equation becomes,

Unknown  
Field Code Changed

Unknown  
Field Code Changed

Unknown  
Field Code Changed

Unknown  
Field Code Changed

478

$$\sigma_Z^2 = \sigma_p^2 \left[ \begin{aligned} & \frac{1}{N} + \frac{2}{N^2} \sum_{i=1}^{N-1} \sum_{j=i+1}^N \exp\left(-v\left((x_i - x_j)^2 + (y_i - y_j)^2\right)^{1/2}\right) \\ & - \frac{2}{NA} \sum_{i=1}^N \int_0^{L_y} \int_0^{L_x} \exp\left(-v\left((x_i - x)^2 + (y_i - y)^2\right)^{1/2}\right) dx dy \\ & + \frac{1}{A^2} \int_0^{L_y} \int_0^{L_x} \int_0^{L_y} \int_0^{L_x} \exp\left(-v\left((x' - x)^2 + (y' - y)^2\right)^{1/2}\right) dx dy dx' dy' \end{aligned} \right] \quad (15)$$

479 The limits of the integrals can be changed depending on the desired location of the origin. In  
 480 this case, the origin is located at the lower-left corner.

481 As discussed earlier, the first term is only a function of  $N$ , such that the base error is the  
 482 variance of the point process divided by the number of points. The second term is a function of  
 483  $N$ , the location of the points, and the decay rate  $v$ . The third term is a function of  $N$ ,  $A$ , the  
 484 location of the points, and the decay rate  $v$ . The fourth term is a function of  $A$  and  $v$ , but is  
 485 independent of the location of the points and  $N$  (i.e., independent of the survey design, and only a  
 486 function of the correlation structure of the continuous process).

### 487 5.1 Case 1: Single measurement in the center of the area

488 In this case, we focus on a single measurement in the middle of a square area of side  
 489 dimension  $L$ . Numerical solution of (15) shows that the normalized squared error increases  
 490 rapidly with  $L$ , with a steeper increase for higher exponential decay exponents (Figure 13a),  
 491 which approach a normalized squared error of 1 for  $L$  values less than 10 (e.g.,  $1 \leq v \leq 5$ ). The  
 492 theoretical results in Figure 13a can be used to determine the discrepancy between a single  
 493 measurement in the middle of an area and the areal mean for a second order stationary and  
 494 anisotropic process with an exponential covariance/correlation function. Comparison of the  
 495 modeled and sampled normalized square errors for the FS snow depth field indicate very good  
 496 agreement between modeled and sample errors (Figure 13b). The sample error is estimated

Unknown  
 Field Code Changed

Ernesto Trujillo 7/4/2015 11:26  
 Formatted: Default Paragraph Font  
 Ernesto Trujillo 7/4/2015 11:26  
 Deleted: (15)



498 following the same procedure explained for the one-dimensional cases, although in the two-  
499 dimensional space. Both sampled and modeled errors show the same behavior across  $L$  values  
500 between 1 m and 100 m, although the scatter in the sampled error increases for larger  $L$  values.  
501 This can be explained by the smaller number of samples to estimate the mean normalized  
502 squared error and the fact that the correlation structure decays rapidly and a single sample  
503 becomes less correlated to the surrounding area for these larger areas. The model introduced here  
504 can then be used to assess the representativeness of a single measurement over an area  
505 objectively and accurately, and it can be extended for other covariance/correlation functions as  
506 needed.

## 507 5.2 Case 2: Five measurements radiating out from the center of the area

508 The case five measurements radiating out from the center (Figure 12a), with a point in the  
509 middle of the area and four points separated by a distance  $a$  from the center leads to a similar  
510 optimization problem as illustrated in case 2 of the one-dimensional examples (section 4.2). In  
511 the two-dimensional case, (15) does not have an explicit solution for  $a$ , and numerical  
512 implementation is required. The equation can be solved by simply replacing the point  
513 coordinates and the correlation function parameters. Following this approach, the normalized  
514 squared error can be obtained for areas of varying sizes (Figure 14). Similar to the one-  
515 dimensional example (case 2, section 4.2),  $\sigma_z^2/\sigma_p^2$  decreases with  $a$ , reaching a minimum at an  
516 intermediate distance from the middle point outwards. The decay in  $\sigma_z^2/\sigma_p^2$  is more rapid for the  
517 least correlated processes (i.e., higher decay exponents) reaching a value close to the base  
518 normalized square error that is a function of the number of points (i.e.,  $1/N = 1/5$  in this case). An  
519 extended analysis of the effect of each of the terms in the equation is included in the

Ernesto Trujillo 2/4/2015 11:44

Deleted: solution that allows for the

Ernesto Trujillo 7/4/2015 11:26

Formatted: Default Paragraph Font

Ernesto Trujillo 7/4/2015 11:26

Deleted: (15)

522 | [Supplementary Information](#). The error, as shown in Figure 14, is minimized as a consequence of  
523 | two balancing terms that lead to this intermediate solution. The optimal solution is a balance  
524 | between reducing the correlation between the individual measurements (e.g., increasing the  
525 | separation between the location of the measurements) but increasing the correlation between the  
526 | measurements and the surrounding area (e.g., locating the measurements closer to the middle of  
527 | the area). These two competing effects lead to an optimization problem based on the location of  
528 | the point measurements. For the least correlated processes, the error behaves closer to the  
529 | behavior of an uncorrelated field once the measurements become effectively decorrelated (e.g.,  $a$   
530 |  $> 1$  in Figure 14b for  $\nu = 5$ ). Figure 14 exemplifies how [\(15\)](#) can be used to determine the  
531 | optimal measurement location for areas of different sizes, and to determine the associated error  
532 | with configurations other than the optimal.

533 | The performance of the model is tested against the normalized squared error obtained from  
534 | the snow depth field in FS. The test consists of estimating the normalized squared error for  
535 | square areas of side dimension ( $L$ ) between 10 m and 79 m, with  $a$  being varied between 0 and  
536 |  $L/2$  (Figure 15). For each value of  $a$ , the normalized squared error is estimated based on the  
537 | means obtained using the five snow depth samples for each section. All squared differences are  
538 | then averaged to obtain the values presented in the [figure](#). Once again, the sampled and modeled  
539 | errors follow the same trend across all  $a$  values and for the different  $L$  values. The minimum  
540 | error and  $a_{optimal}$  are also reproduced closely by the model, and as the area size increases, the  
541 | sampled and modeled error approach the error for an uncorrelated field at larger separations (i.e.,  
542 | 0.2). These results illustrate that the performance of the model in the two-dimensional space is  
543 | remarkable, similar to what was observed in the one-dimensional case.

Ernesto Trujillo 7/4/2015 11:26

Formatted: Default Paragraph Font

Ernesto Trujillo 7/4/2015 11:26

Deleted: (15)

Ernesto Trujillo 1/4/2015 18:07

Deleted: Figure

546 **5.3 Case 3:  $N$  by  $N$  measurements regularly spaced in the  $x$  and  $y$  directions**

547 Similarly to the one-dimensional case, the two-dimensional case of  $N$  by  $N$  regularly spaced  
548 measurements (Figure 12b) leads to a decreasing normalized squared error with  $N$  (Figure 16).  
549 There is a sharp decrease in the error with just increasing the number of measurements in the  
550 lower range of  $N$ . The analysis illustrates that stratified sampling, as the one shown here, is an  
551 excellent approach to minimizing the error. For example, for the area of 10 by 10, increasing  $N$   
552 to 4 ( $N^2 = 16$ ) reduces the normalized squared error to less than 0.05. It is also worth noting here  
553 that for this two-dimensional case, the error is less sensitive to the value of the exponential decay  
554 exponent ( $\nu$ ) for the higher  $N$  values as the mean is accurately captured regardless of the  
555 correlation of the field. Beyond a certain number of measurements regularly distributed in the  
556 area, the measurements gather enough information such that there are only very minor  
557 improvements with the addition of new measurements, regardless of the exponent value. Figure  
558 16 serves as an example of how the methodology can be used for objective selection of the  
559 number of measurements necessary to achieve a desired accuracy level using prior knowledge of  
560 the spatial covariance function.

561 The performance of the model is tested again for square areas of side dimension ( $L$ ) between  
562 10 m and 79 m using the snow depth field in FS, and for an increasing number of rows/columns  
563 of measurements leading to a total number of measurements of  $N^2$  (Figure 17). The results  
564 illustrate again the accurate performance of the theoretical model, with sampled and model errors  
565 following closely the same squared errors. Both sampled and modeled errors increase as the size  
566 of the area increases, as expected. These results complete the model performance tests for the  
567 two-dimensional isotropic case.

568

## 6 Summary and Conclusions

569 A methodology for an objective evaluation of the error in capturing mean snow depths from  
570 point measurements is presented based on the expected value of the squared difference between  
571 the real average snow depth and the mean of a finite number of snow depth samples within a  
572 defined domain (e.g., a profile section or an area). The model can be used for assisting the design  
573 of survey strategies such that the error is minimized in the case of a limited and predetermined  
574 number of measurements, or such that the desired number of measurements is determined based  
575 on a predefined acceptable uncertainty level. The model is applied to one- and two-dimensional  
576 survey examples using LIDAR snow depths collected in the Colorado Rockies. The results  
577 confirm that the model is capable of reproducing the estimation error of the mean from a finite  
578 number of samples for real snow depth fields.

579 Here, we should highlight some of the implications of the assumptions made in the model. In  
580 simplified terms, the second-order stationarity assumption implies that the mean and the variance  
581 of the process/variable (e.g., snow depth) are independent of the spatial location, and that the  
582 covariance is dependent only on the separation vector (i.e., lag). Although these assumptions  
583 may not be as adequate over larger scales (e.g., greater than 100 m), at smaller scales the  
584 assumption in the context of the model application to snow depth should be valid. We present  
585 these examples to show how the error can be quantified with good accuracy around such smaller  
586 scales. Application of such types of approaches at larger scales will require additional  
587 evaluations with particular attention as to what the specific demands of the application are. Also,  
588 the methodology as presented here is not suitable for discontinuous snow covers if both snow-  
589 covered and snow-free areas are considered in the error estimation. This case has not been  
590 considered in the development here.

591 Implementation of the model in practice requires prior assumption of a  
592 correlation/covariance model and estimates of the parameters of this model (e.g., the decay  
593 exponent for the exponential case). In the examples here we use LIDAR data for the parameter  
594 estimation, which we have done to illustrate the applicability of the model and its ability to  
595 estimate the error using real snow depth data. Snow distribution in mountain environments has  
596 been shown to be consistent intra- and inter-annually because the controlling processes are  
597 relatively consistent during the season and from season to season. Such consistency suggests that  
598 the correlation/covariance model should also be consistent, as well as the parameters of the  
599 model. These parameters can be estimated via a dense survey either manually or with TLS of one  
600 or more small plots of a size similar to the size that is aimed to be represented. These surveys  
601 would not necessarily have to be repeated as the parameters and covariance models should be  
602 preserved. Detailed surveys can be conducted under different conditions to characterize the range  
603 of the correlation models and parameters (e.g., after a snow storm, or close to peak  
604 accumulation). Also here, we should point out that although we show results for a wide range of  
605 the exponential decay exponent values, we are finding that most of the values that we have  
606 observed are in the lower range of those presented (e.g.,  $0.1-0.2 \text{ m}^{-1}$ ). Hence, the biases in the  
607 estimated error and the survey design remain small.

608 Currently, remote sensing technologies (e.g., TLS, Airborne LiDAR, and ground penetrating  
609 radar) are allowing for the characterization of snow cover properties at increasing resolutions in  
610 both space and time. Such improvements can be utilized in the context presented here providing  
611 information about the range of best fitting covariance/correlation models and parameters for  
612 different conditions, supporting the application of methodologies such as the one presented here.  
613 With such improvements, survey designs can be optimized such that estimation errors can be

Ernesto Trujillo 27/3/2015 17:35

**Deleted:** These properties are also shared by other spatially heterogeneous fields and processes that are hydrologically-relevant, such as snow water equivalent, soil moisture and precipitation, among others. In consequence, this methodology can be extended to the aforementioned variables and processes.

Ernesto Trujillo 30/3/2015 14:59

**Deleted:** Ground

Ernesto Trujillo 30/3/2015 14:59

**Deleted:** Penetrating

Ernesto Trujillo 30/3/2015 14:59

**Deleted:** Radar

Ernesto Trujillo 30/3/2015 14:50

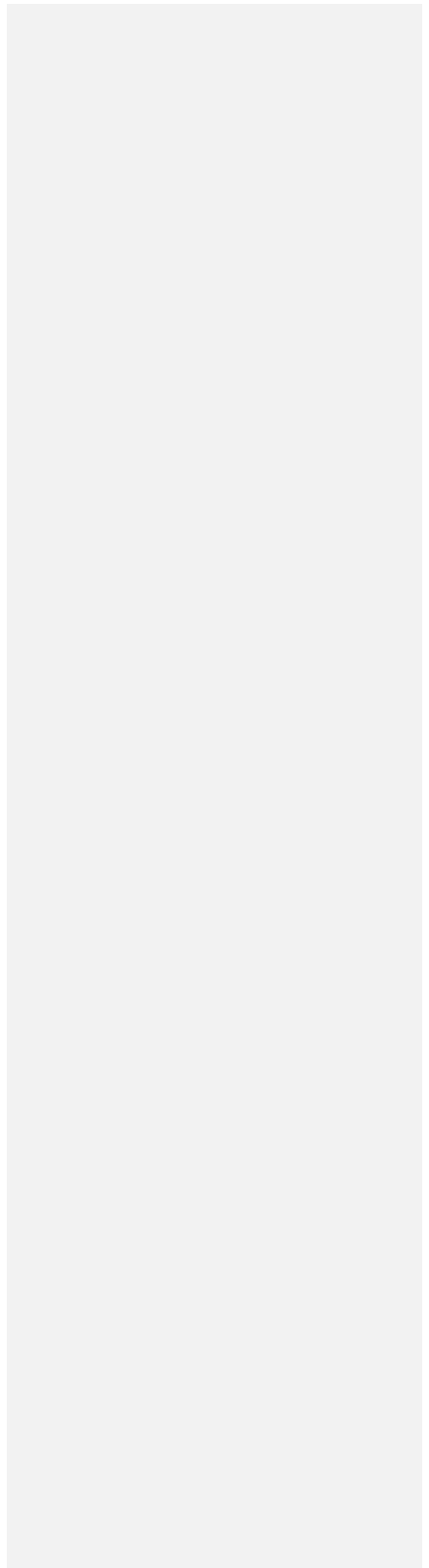
**Deleted:** introduced

Ernesto Trujillo 30/3/2015 14:55

**Deleted:** here to optimize

626 explicitly addressed and accounted for, particularly when extrapolating a limited number of  
627 measurements to estimate the spatial distribution of snow. Such applications will continue to be  
628 relevant despite of the aforementioned improvements, as access to these technologies is limited  
629 | by their cost and the expertise that is required for their application.

630



631

632

## **7 Acknowledgements**

633

Data for this article was obtained from NASA's Cold Land Processes experiment (CLPX),

634

available at [http://nsidc.org/data/docs/daac/nsidc0157\\_clpx\\_lidar](http://nsidc.org/data/docs/daac/nsidc0157_clpx_lidar).

635

## Figures

638 Figure 1. (a) Location of the Fraser and Rabbit Ears study areas in the state of Colorado (in  
639 grey). (b) LIDAR Snow depth distributions on April 8, 2003, at the Saint Louis Creek Intensive  
640 Study Area (ISA) and (c) on April 9 at the Rabbit Ears ISA.

641 Figure 2. (a) Sample normalized snow depth profile (mean = 0, standard deviation = 1) in a  
642 forested environment from LIDAR (1-m resolution) at the Fraser – St. Louis Creek (FS)  
643 intensive study area (ISA) of the Cold Land Processes eXperiment (CLPX) (Trujillo et al., 2007;  
644 Cline et al., 2009). The profile is sampled with regular separations (spacing) of 5 m, 10 m, 25 m,  
645 50 m, and 100 m (from top to bottom, respectively). (b) Average values within sampling  
646 intervals (same as in (a)) versus point samples for normalized snow depth profiles in the FS ISA.  
647 The red line is a linear regression fit, with slope  $\beta$  and  $r^2$  as indicated in each plot. (c) Histograms  
648 of the difference between the point and average values for each of the sampling intervals. The  
649 vertical red line marks the mean difference.

650 Figure 3. (a) As Figure 2 but for an open and wind **influenced** environment at the Rabbit Ears  
651 – Walton Creek (RW) ISA of the CLPX (Trujillo et al., 2007; Cline et al., 2009). (b) Average  
652 values within sampling intervals (same as in (a)) versus point samples for normalized snow depth  
653 profiles in the RW ISA. The red line is a linear regression fit, with slope  $\beta$  and  $r^2$  as indicated in  
654 each plot. (c) Histograms of the difference between the point and average values for each of the  
655 sampling intervals. The vertical red line marks the mean difference.

656 Figure 4. Sub-interval standard deviation (a) and range (b) for varying interval lengths for  
657 profiles of snow depth in a forested environment (FS) and an open and wind-influenced  
658 environment (RW) in the Colorado Rocky Mountains (same regions as those in Figure 2 and  
659 Figure 3). The mean standard deviation and mean range for the study areas are shown by the  
660 solid lines, while the shaded areas cover the quantiles between 25% and 75% of the values for all  
661 the intervals in these areas.

662 Figure 5. Survey designs for the sampling of a snow profile.

663 Figure 6. Comparison of the theoretical and sampled normalized squared error ( $\sigma_z^2/\sigma_p^2$ ) for  
664 the case of a single measurement along a profile section of length  $L$ , as in Figure 5a. The survey  
665 case applied to profiles in FS and RW along the  $x$  and  $y$  directions. Solid lines are the theoretical  
666 error using exponential decay exponents derived from the functions fitted to the sampled  
667 correlation functions of the two surfaces in the  $x$  and  $y$  directions.

668 Figure 7. (a) Theoretical normalized squared error for a single measurement in the middle of a  
669 section of length  $L$ , and for an exponential correlation function with a decay exponent,  $v$ . (b) and  
670 (c) Comparison of the theoretical and sampled normalized squared error for the same survey case  
671 applied to profiles in FS and RW along the  $x$  and  $y$  directions. Dashed lines are the theoretical  
672 error from (7) using exponential decay exponents derived from the functions fitted to the  
673 sampled correlation functions of the two surfaces in the  $x$  and  $y$  directions.

674 Figure 8. (a) and (b) Theoretical normalized squared error for the three-point pattern along a  
675 profile section in Figure 5b, and for profile section lengths ( $L$ ) of 1 (a) and 25 (b). Each of the

Ernesto Trujillo 1/4/2015 18:18

Deleted: dominated



677 colored lines corresponds to a specific decay exponent,  $\nu$ , and the black line marks the  
678 theoretical solution for  $a_{optimal}$ . (c) Theoretical normalized error and  $a_{optimal}$  for isolines of profile  
679 section lengths ( $L$ ) and exponential decay exponents ( $\nu$ ) for the three-point pattern along a profile  
680 section of length  $L$  in Figure 5b.

681 Figure 9. Theoretical and sampled normalized squared error ( $\sigma_z^2/\sigma_p^2$ ) for the three-point  
682 pattern along a profile section in Figure 5b, and for profile section lengths ( $L$ ) between 10 m and  
683 80 m in FS and RW. The solid lines are the theoretical error from (8) using exponential decay  
684 exponents derived from the functions fitted to the sampled correlation functions of the two  
685 surfaces in the  $x$  and  $y$  directions, while the dots correspond to the sampled error for profiles in  
686 FS (a-d) and RW (e-h).

687 Figure 10. Theoretical normalized squared error ( $\sigma_z^2/\sigma_p^2$ ) for the  $N$ -point pattern along a  
688 profile section in Figure 5c, and for profile section lengths ( $L$ ) between 10 and 80 obtained from  
689 (10).

690 Figure 11. Theoretical and sampled normalized squared error ( $\sigma_z^2/\sigma_p^2$ ) for the  $N$ -point pattern  
691 along a profile section in Figure 5c, and for profile section lengths ( $L$ ) between 10 m and 80 m in  
692 FS and RW. The solid point markers are the theoretical error from (10) using exponential decay  
693 exponents derived from the functions fitted to the sampled correlograms of the two surfaces in  
694 the  $x$  and  $y$  directions, while the circle markers with the dotted lines correspond to the sampled  
695 error for profiles in FS (a-d) and RW (e-h).

696 Figure 12. Sample survey designs with (a) a 5-point pattern centered in the area, and (b) a  
697 regularly spaced pattern. For the 5-point pattern,  $a$  can vary between 0 and  $L/2$ , while for the  $N \times$   
698  $N$  points pattern, the separation between the measurements is determined by the number of  
699 points.

700 Figure 13. (a) Theoretical normalized squared error ( $\sigma_z^2/\sigma_p^2$ ) for the two-dimensional case  
701 with a single measurement in the middle of a square area with side dimension  $L$ . (b) Theoretical  
702 and sampled normalized squared error for the same two-dimensional survey applied to the snow  
703 depth field in FS. The dashed line is the theoretical error derived for an exponential decay  
704 exponent of 0.17 derived from the sampled correlation function of snow depth in FS, while the  
705 solid line is the sampled normalized squared error for the snow cover in FS.

706 Figure 14. Theoretical normalized squared error ( $\sigma_z^2/\sigma_p^2$ ) as a function of the distance  $a$  from  
707 the center of the area for square areas of side dimensions ( $L$ ) between 10 and 80. Each curve  
708 corresponds to an exponential decay ( $\nu$ ) between 0.1 and 5.

709 Figure 15. Theoretical and sampled normalized squared error ( $\sigma_z^2/\sigma_p^2$ ) for the 5-point pattern  
710 in Figure 12a over square areas of side dimensions ( $L$ ) between 10.7 m and 79.1 m. The  
711 separation distance ( $a$ ) is varied from the center outwards. The solid line is the theoretical error  
712 derived for an exponential decay exponent of 0.17 derived from the sampled correlation function  
713 of snow depth in FS, while the solid red point markers are the sampled normalized squared error  
714 for the snow cover in FS.

715 Figure 16. Theoretical normalized squared error ( $\sigma_z^2/\sigma_p^2$ ) for the  $N$  by  $N$  point pattern in  
716 Figure 12b, and for areas of side dimension ( $L$ ) between 10 and 80. The exponential exponent is  
717 varied between 0.1 and 5.

718 Figure 17. Theoretical and sampled normalized squared error ( $\sigma_z^2/\sigma_p^2$ ) for the  $N$  by  $N$  point  
719 pattern in Figure 12b, and over square areas of side dimensions ( $L$ ) between 10.7 m and 79.1 m.  
720 The solid black point markers are the theoretical error for an exponential decay exponent of 0.17  
721 derived from the sampled correlogram of snow depth in FS. The dotted red lines with circle  
722 markers are the sampled normalized squared error for the snow cover in FS.

723

724

- 726 Blöschl, G.: Scaling issues in snow hydrology, *Hydrol. Processes*, 13(14-15), 2149-2175, 1999.
- 727 Chang, A. T. C., Kelly, R. E. J., Josberger, E. G., Armstrong, R. L., Foster, J. L., and Mognard,  
728 N. M.: Analysis of ground-measured and passive-microwave-derived snow depth variations in  
729 midwinter across the northern Great Plains, *J. Hydrometeor.*, 6(1), 20-33, doi: 10.1175/Jhm-  
730 405.1, 2005.
- 731 Cline, D., Yueh, S., Chapman, B., Stankov, B., Gasiewski, A., Masters, D., Elder, K., Kelly, R.,  
732 Painter, T. H., Miller, S., Katzberg, S., and Mahrt, L.: NASA Cold Land Processes Experiment  
733 (CLPX 2002/03): Airborne Remote Sensing, *J. Hydrometeor.*, 10(1), 338-346, 2009.
- 734 Cressie, N.: *Statistics for spatial data*, 900 pp., John Wiley & Sons, Inc., USA, 1993.
- 735 Deems, J. S., Fassnacht, S. R., and Elder, K. J.: Interannual Consistency in Fractal Snow Depth  
736 Patterns at Two Colorado Mountain Sites, *J. Hydrometeor.*, 9(5), 977-988, doi:  
737 10.1175/2008jhm901.1, 2008.
- 738 Grünewald, T., and Lehning, M.: Are flat-field snow depth measurements representative? A  
739 comparison of selected index sites with areal snow depth measurements at the small catchment  
740 scale, *Hydrol. Processes*, doi: 10.1002/hyp.10295, 2014.
- 741 Helfrich, K., Schöber, J., Schneider, K., Sailer, R., and Kuhn, M.: Interannual persistence of the  
742 seasonal snow cover in a glacierized catchment, *J. Glaciol.*, 60(223), 889-904, doi:  
743 10.3189/2014JoG13J197, 2014.
- 744 Journel, A. G., and Huijbregts, C. J.: *Mining Geostatistics*, Academic Press, London, 1978.
- 745 Kronholm, K., and Birkeland, K. W.: Reliability of sampling designs for spatial snow surveys,  
746 *Comput. Geosci.*, 33(9), 1097-1110, 2007.
- 747 Lopez-Moreno, J. I., Fassnacht, S. R., Begueria, S., and Latron, J. B. P.: Variability of snow  
748 depth at the plot scale: implications for mean depth estimation and sampling strategies,  
749 *Cryosphere*, 5(3), 617-629, 2011.
- 750 Matheron, G.: Application des méthodes statistiques à l'estimation des gisements, *Annales de*  
751 *Mines, Dec*, 50-75, 1955.
- 752 Matheron, G.: Random functions, and their applications in geology, in *Geostatistics - A*  
753 *colloquium*, edited by D. Merriam, pp. 79-87, Plenum Press, New York, 1970.
- 754 Melvold, K., and Skaugen, T.: Multiscale spatial variability of lidar-derived and modeled snow  
755 depth on Hardangervidda, Norway, *Ann. Glaciol.*, 54(62), 273-281, 2013.
- 756 Meromy, L., Molotch, N. P., Link, T. E., Fassnacht, S. R., and Rice, R.: Subgrid variability of  
757 snow water equivalent at operational snow stations in the western USA, *Hydrol. Processes*,  
758 27(17), 2383-2400, doi: 10.1002/Hyp.9355, 2013.
- 759 Mott, R., Schirmer, M., and Lehning, M.: Scaling properties of wind and snow depth distribution  
760 in an Alpine catchment, *Journal of Geophysical Research: Atmospheres*, 116(D6), D06106, doi:  
761 10.1029/2010jd014886, 2011.

762 Rice, R., and Bales, R. C.: Embedded-sensor network design for snow cover measurements  
763 around snow pillow and snow course sites in the Sierra Nevada of California, *Water Resour.*  
764 *Res.*, *46*, W03537, doi: 10.1029/2008wr007318, 2010.

765 Rodríguez-Iturbe, I., and Mejía, J. M.: Design of Rainfall Networks in Time and Space, *Water*  
766 *Resour. Res.*, *10*(4), 713-728, 1974.

767 Schirmer, M., Wirz, V., Clifton, A., and Lehning, M.: Persistence in intra-annual snow depth  
768 distribution: 1. Measurements and topographic control, *Water Resour. Res.*, *47*(9), W09516, doi:  
769 10.1029/2010wr009426, 2011.

770 Shea, C., and Jamieson, B.: Star: an efficient snow point-sampling method, *Ann. Glaciol.*,  
771 *51*(54), 64-72, 2010.

772 Skøien, J. O., and Blöschl, G.: Sampling scale effects in random fields and implications for  
773 environmental monitoring, *Environ. Monit. Assess.*, *114*(1-3), 521-552, doi: Doi  
774 10.1007/S10661-006-4939-Z, 2006.

775 Sturm, M., and Wagner, A. M.: Using repeated patterns in snow distribution modeling: An  
776 Arctic example, *Water Resour. Res.*, *46*, 2010.

777 Trujillo, E., Ramirez, J. A., and Elder, K. J.: Topographic, meteorologic, and canopy controls on  
778 the scaling characteristics of the spatial distribution of snow depth fields, *Water Resour. Res.*, *43*,  
779 W07409, doi: 10.1029/2006WR005317, 2007.

780 Trujillo, E., Ramirez, J. A., and Elder, K. J.: Scaling properties and spatial organization of snow  
781 depth fields in sub-alpine forest and alpine tundra, *Hydrol. Processes*, *23*, 1575-1590, doi:  
782 10.1002/hyp.7270, 2009.

783 Watson, F. G. R., Anderson, T. N., Newman, W. B., Alexander, S. E., and Garrott, R. A.:  
784 Optimal sampling schemes for estimating mean snow water equivalents in stratified  
785 heterogeneous landscapes, *J. Hydrol.*, *328*(3-4), 432-452, doi: 10.1016/J.jhydrol.2005.12.032,  
786 2006.

787 Yang, D. Q., and Woo, M. K.: Representativeness of local snow data for large scale hydrologic  
788 investigations, *Hydrol. Processes*, *13*(12-13), 1977-1988, doi: 10.1002/(Sici)1099-  
789 1085(199909)13:12/13<1977::Aid-Hyp894>3.0.Co;2-B, 1999.

790

791